UNCLASSIFIED
SECURITY CLASSIFICATION OF THIS PAGE (When Data Entered)

AD A109056

REPORT DOCUMENTATION PAGE

READ INSTRUCTIONS BEFORE COMPLETING FORM

1. REPORT NUMBER: AFOSR-TR- 81-0859	2. GOVT ACCESSION NO.: AD-A109 056
3. RECIPIENT'S CATALOG NUMBER:	
4. TITLE (and Subtitle): Report on the Analysis of Data from the NOAA/ Alaskan MST Radar System	5. TYPE OF REPORT & PERIOD COVERED: Interim
	6. PERFORMING ORG. REPORT NUMBER:
7. AUTHOR(s): M. F. Larsen, M. C. Kelley, and D. T. Farley	8. CONTRACT OR GRANT NUMBER(s): AFOSR-30-0020
9. PERFORMING ORGANIZATION NAME AND ADDRESS: Cornell University, School of Electrical Engineering, Ithaca, NY 14853	10. PROGRAM ELEMENT, PROJECT, TASK AREA & WORK UNIT NUMBERS: 61102F, 2310/A1
11. CONTROLLING OFFICE NAME AND ADDRESS: Air Force Office of Scientific Research/NC, Bolling AFB, DC 20332	12. REPORT DATE: November 1981
	13. NUMBER OF PAGES: 40
14. MONITORING AGENCY NAME & ADDRESS (if different from Controlling Office): LEVEL II	15. SECURITY CLASS. (of this report): Unclassified
	15a. DECLASSIFICATION/DOWNGRADING SCHEDULE:

16. DISTRIBUTION STATEMENT (of this Report)

Approved for public release; distribution unlimited.

DTIC ELECTE DEC 3 1 1981 S D H

17. DISTRIBUTION STATEMENT (of the abstract entered in Block 20, if different from Report)

18. SUPPLEMENTARY NOTES

19. KEY WORDS (Continue on reverse side if necessary and identify by block number)

Geostrophic Winds	Radar Winds
Cressman Analysis	Objective Analysis
Gandin Analysis	Atmospheric Power Spectra
MST Radar	Turbulence

20. ABSTRACT (Continue on reverse side if necessary and identify by block number)

During this period the investigation of mesoscale eddy spectra was completed as well as a study of objective analysis schemes using geostrophic wind adjustments. Both depend upon the continuous data of the NOAA MST radar at Poker Flat, Alaska. The atmospheric power spectral studies revealed a k to the minus 5/3 inertial subrange at time scales of hours. The implication in this essentially two dimensional eddy regime is a source of energy existing at spatial scales of less than 100 km, progagating energy up the spectrum

DD FORM 1 JAN 73 1473 EDITION OF 1 NOV 65 IS OBSOLETE

UNCLASSIFIED
SECURITY CLASSIFICATION OF THIS PAGE (When Data Entered)

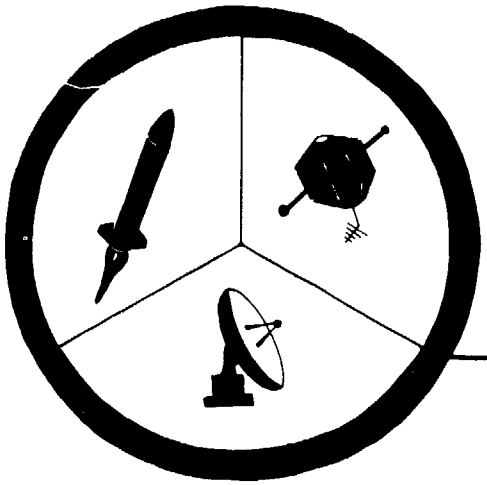

ATMOSPHERE
IONOSPHERE
MAGNETOSPHERE

REPORT ON THE ANALYSIS OF DATA FROM THE NOAA/ALASKAN MST RADAR SYSTEM

Second Progress Report for

Grant AFOSR-80-0020

M.F. Larsen

M.C. Kelley

D.T. Farley

November 1981

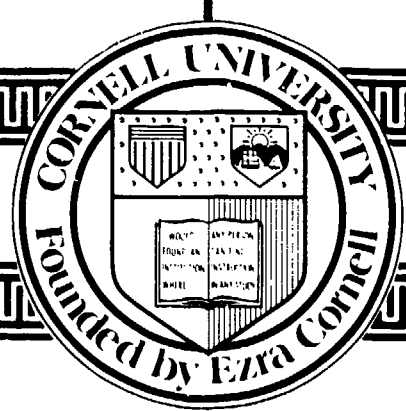

CORNELL UNIVERSITY

SCHOOL OF ELECTRICAL ENGINEERING
ITHACA, NEW YORK 14853

toward lower wavenumbers. At smaller scales, in the fully 3-D turbulent spectrum, the classic kolmogorov inertial spectrum is found with energy cascading towards smaller scales. Again, a source of energy is suggested on the scale of 10-100 km. The candidate is convection. In the study of objective analysis techniques, Cressman, Gandin and other approaches are analysed using the continuous radar data record. No significant differences were found between the Cressman and Gandin schemes. Knowing the character of the radar data with respect to these well-known analyses now permits comparison to more sophisticated and less trivial techniques and may lead to suggestions for entirely new concepts.

PROGRESS REPORT FOR GRANT AFOSR-80-0020

November 1981

Introduction

During the past year of research under Air Force grant AFOSR-80-0020 we have finished our investigation of large-scale turbulence at periods characterizing the meteorological mesoscale, and we have now completed the first part of a study of the validity of various objective analysis schemes. Both of these projects involve the analysis of data from the NOAA M-S-T (Mesosphere/ Stratosphere/Troposphere) radar located at Poker Flat, Alaska. The details of the system have been described by Gage and Balsley [1978], Balsley et al. [1980], and Balsley and Gage [1980]. The data used in our project consists of high time resolution data, one profile every 4 min., for six different heights in the troposphere and lower stratosphere, averaged over one-hour intervals. This type of data was not available from any other source prior to the M-S-T radar and has provided the opportunity to carry out some unique investigations of importance to synoptic meteorology.

Investigation of Turbulence at the Meteorological Mesoscale

Forty days of horizontal wind data from the radar were used to investigate turbulence in the upper troposphere and lower stratosphere at periods between 2 hours and 40 days. The power spectra of the winds showed a $k^{-5/3}$ inertial subrange at time scales characteristic of the mesoscale. Various arguments can be used to show that for the time scales in question the flow is two-dimensional (see Appendix I). The implication is that a source of energy exists at spatial scales less than 100 km, propagating energy up the spectrum toward lower wavenumbers. A candidate for this source of energy is the release of latent heat associated with convection.

The results of this part of the study which has now been completed are described in detail in the paper reproduced in Appendix I. The paper has been submitted to J. Atmos. Sci. and has gone through the refereeing process. The paper was deemed to qualify for "probable acceptance after revisions."

Investigation of Objective Analysis Schemes

Since the observations of the meteorological data network are irregularly spaced and of variable density in various parts of the globe, some technique has to be used to interpolate the observations to a regular grid that can be used as input for a numerical forecast model. Because the interpolation problem is such a basic part of numerical weather forecasting, schemes to accomplish this have existed as long as the numerical models. The first objective analysis algorithm to gain wide acceptance was that formulated by Cressman [1959]. It was computationally efficient and seemed to provide good agreement with the results of subjective analyses of the same data fields and was used by the National Meteorological Center for many years. Since then the Cressman technique has been expanded upon by various people who have tried to include more of the actual physics of the atmosphere in their particular objective analysis method. Some of these have been reviewed by Kruger [1969], and others were described by Otto-Bliesner et al. [1977].

The goal of all objective analysis procedures is to generate a value of the meteorological variable in question that is representative of the true value at the grid point based on observations at a cluster of points around the grid point. The interpolated values are also required to be in a balanced state such as that represented by the geostrophic wind. The second condition is imposed to avoid generating spurious waves once the model is initialized. Since the balance condition is an integral part of objective analysis, it provides a check on the validity of the various schemes, particularly if a good estimate of the balanced wind is available.

Verification of the validity of the various objective analysis methods has always been difficult. As an example, we can consider the method used by Kruger [1969] who was interested in evaluating the differences between the methods of Cressman [1959], Gandin [1963], and the Central Analysis Office of

Canada [Kruger and Asselin, 1967]. Each of these schemes uses a weighting function which only depends on radial distance from the grid point. An obvious choice for the weighting is the autocorrelation function for the meteorological variable in question. In fact, Cressman's and Gandin's schemes use approximations for the autocorrelation function, and the Central Analysis Office method actually calculates the autocorrelation from past data. To test the validity of the different methods, Kruger [1969] compared the maps generated by applying the schemes to maps generated by a subjective analysis of a 500 mb height field. A similar technique has been used to test other schemes [see e.g., Otto-Bliesner et al., 1977]. Of course, this merely tests the ability of the objective analysis routine to produce an analysis in agreement with that produced subjectively by the meteorologist. It is not a test of the ability of the routine to produce values corresponding to the real state of the atmosphere. In fact, Otto-Bliesner et al. [1977] found that the various schemes tended to agree more with each other than with the subjective analysis.

Due to the large uncertainties in the winds determined by the radiosonde data network, it has been difficult to test the objective analysis methods by means other than those described above. Since the balloons obtain a snapshot profile of the winds, they are likely to be contaminated by oscillations of relatively high frequency compared to the synoptic scale motions of interest in the numerical models. The Poker Flat M-S-T (Mesosphere/Stratosphere/Troposphere) radar has provided an independent set of wind data that can be used to provide a test of the objective analysis procedures described above. The radar obtains a wind profile once every 4 minutes. By averaging these over longer time intervals, the higher frequency oscillations can be eliminated from the data, and a good estimate of the quasi-steady wind is possible.

In our study to date we have investigated three different analysis

methods. A forty day period from February 28 to April 5, 1979 when the horizontal winds measured by the radar are available was used together with the standard radiosonde data for 00Z and 12Z during this period to study the agreement between the radar winds and the geostrophic wind predicted by an objective analysis of the observed height field. The distribution of stations and their location relative to Poker Flat are shown in Figure 1. The station furthest from Poker Flat is Yakutat located 764 km from the site of the radar. Barter Island is 572 km away, McGrath 476 km, and Anchorage 455 km. The closest radiosonde station is Fairbanks which is 36 km SSE of Poker Flat. An analysis which uses five stations is usually considered good, especially if the stations are within a radius of 1500 to 2500 km of the grid point of interest [Kruger, 1969].

The algorithms for the various schemes can all be formulated in the same way as

$$f_g^I = R_g + \sum_{i=1}^{n} C_i^f f_i^o + \sum_{j=1}^{m} C_j^s (S_j^o)_g \qquad (1)$$

where f_g^I is the interpolated value at the grid point g, R_g is an initial guess of the value of f_g^I, f_i^o is the observed value of f at observation point i, and S_j^o is an observed variable that can be used to infer the value of f. For instance, S_j^o could be the wind field if f is the height field. The C's are the weights given to each of the observed values. Different objective analysis schemes change the way that the different weights or initial guesses are specified, but otherwise (1) is perfectly general.

For all our calculations the objective analysis scheme was applied to the observations to provide values of the height field at five grid points. One grid point coincides with the location of Poker Flat. The other four are distributed so that they are located one each at a distance 100 km north,

south, east, and west of Poker Flat. The initial guess for the height field at each of the grid points was found from the average value of the height over the forty day period at each of the observation points. The three closest stations to any one grid point were used to calculate the horizontal gradient of the height field, and this value of the gradient was then used to calculate an expected value at the grid point. This procedure falls into the category of using climatology as an initial guess. A variant on this is to use the forecast output from a numerical model as the initial guess. However, this option was not available to us since we did not have a model for that purpose.

Although we have carried out an analysis of the height fields, which is standard in meteorology, there is one slight variation. For the forty day period that we are discussing, the radar was getting a fairly continuous stream of data at six or seven heights in the upper troposphere and lower stratosphere. Since the range gates of the radar are fixed, it was not possible to vary the height of the measurement to correspond to a standard pressure level. To circumvent this problem, the pressure at the height of the radar measurement was calculated from the Fairbanks radiosonde data. The height corresponding to this pressure was then found for each of the other observing stations. This should not make any difference in carrying out the 12-hourly objective analysis since this is independent of previous values. This can only affect the determination of the climatological averages for the period. The average becomes the average height at each of the observing points corresponding to the pressure at a fixed height over Poker Flat. In any case, the agreement between the measured winds and the geostrophic winds calculated from the height field improved substantially when the initial guess field was included as will be seen later.

The first method that we investigated was that developed by Cressman [1959] and used at the National Meteorological Center for a number of years.

Referring back to (1), it corresponds to the case in which $C_j^s=0$ and C_i^f is given by

$$C_i^f = \frac{1}{n}\frac{(R^2-D^2)}{(R^2+D^2)} \tag{2}$$

where R is the radius of influence and D is the distance between the grid point and the observation. The factor n is the total number of stations used in the analysis for one individual grid point. The weighting is zero if D>R. The weighting function is shown as the curve labelled CR1 in Figure 2. The second method investigated is that represented by the weighting function labelled GANDIN in Figure 2. The third curve labelled CAO is the autocorrelation curve calculated from past data by the Central Analysis Office of Canada. The real autocorrelation becomes negative beyond 1500 km whereas the Cressman and Gandin curves never become negative. The Gandin curve is a Gaussian, and the Cressman curve is zero by definition beyond the radius of influence.

The effect of not including a good initial guess of the height values at the grid points can be seen by comparing Figures 3a and 3b. Both represent the result of a Cressman analysis with a radius of influence of 1,000 km. The heights are indicated in the lower left-hand corner of each frame. The agreement between the calculated and measured winds is indicated by sigma which is the standard error given by

$$\sigma = \frac{1}{n-1}\left(\sum_{i=1}^{n}(v_i-\tilde{v}_i)\right)^{\frac{1}{2}} \tag{3}$$

Here n is the number of points in the time series, v_i is the measured value of the wind, and $\tilde{v}_i$ is the geostrophic wind calculated from the height field. Approximately 63% of the measured values will lie within $\pm\sigma$ of the estimated

value. For the case with no initial guess large errors occur in the zonal component in particular. The error is reduced by a little over 8 m/s at the worst height which is 10.39 km when the initial guess is included. There is no significant difference in the meridional component when the initial guess is omitted. It is evident that the initial guess just establishes a base level. The objective analysis scheme then determines the variation about that level on a given day. Thus the errors are larger in the zonal component which has a larger mean wind than the meridional component. The error is also larger at 10.39 km which corresponds to the peak in the mean wind as a function of height.

Certain general features which are evident in Figure 3b are noteworthy because they persist in all the various analyses that are presented here. The smallest standard error is at the lowest height for which we have data, namely 3.79 km. The largest error occurs at 8.19 km and 10.32 km. These heights are also in the range where the largest mean winds occur. Finally, the error begins to decrease with increasing altitude in the stratosphere.

The smallest error variance was found to occur for a radius of influence of 750 km, although the difference between using a radius of influence of 1,000 km and 750 km was less than 0.5 m/s at all heights. However, the difference between a radius of influence of 2,000 km and one of 750 km was to increase the error by 1 to 3 m/s. This is shown in Figure 3c.

The Gandin method with its Gaussian weighting gave the best results when a radius of influence, i.e., a Gaussian half-width, of 500 km was used. The result is shown in Figure 3d. The errors were consistently larger than the best case for the Cressman analysis. However, the difference between the two was insignificant, being no greater than 0.4 m/s.

For the results described above, the analysis method has been varied and a 12-hour average of the radar winds has been used as a comparison. The effect

of increasing the averaging interval is to decrease the error. This can be seen in Figure 3e which shows a 48-hour average of the radar winds compared to the Cressman analysis with a radius of influence of 1,000 km. Comparison with the 12-hour average results shown in Figure 3b shows that the error has been reduced by as much as 4 m/s at 8.19 km in the zonal component. The error has not been substantially reduced in the meridional component. As the averaging interval increases beyond 12 hours, the error in the meridional component stays relatively constant. The error in the zonal component continues to decrease. This could be explained by a series of wave perturbations propagating on a zonal current.

The actual scheme described by Cressman [1959] involved using the weighting function that we have described above together with a series of successive scans to improve the estimate of the interpolated grid-point value. In a series of five successive scans the radius of influence is reduced by 20% of its original value. Thus only the closest stations influence the corrections applied on the last scan. The result of application of this method is shown in Figure 3f. Although the method produces quite a few more oscillations in the pressure field, making it appear as variable as the wind field, the overall effect is to increase the error.

As a standard for comparison, Figure 3g shows the result of calculating the geostrophic winds using the observed heights at Anchorage, McGrath, and Fairbanks. These three stations were chosen because they are nearest to Poker Flat. The winds calculated in this way have a strong oscillation between successive 12 hourly values. Therefore a 3 point, equally weighted moving average was applied to the radiosonde-derived winds. When compared to the 1,000 km Cressman analysis shown in Figure 3b, the error at stratospheric heights is actualy smaller when the three-station method is used. Below the tropopause the Cressman method gives better agreement.

The only other study that we are aware of that has investigated the geostrophy of the wind is the one by Angell [1959]. He used data from a constant level balloon (transosonde) at 300 mb. The winds were derived by using the change in position of the balloon over 8 hours. The curves presented by Angell correspond to a standard error of approximately 12 m/s. The 300 mb level is close to 9-km altitude. At 8.19 km and 10.39 km the standard error for the Cressman analysis compared to a 12 hour average of the radar winds was 10.69 and 10.32 m/s respectively. Although these values are smaller, they compare favorably with the values calculated by Angell.

We have found that there is no significant difference between the Cressman and Gandin objective analysis schemes. Although the magnitude of the ageostrophic wind component increases when the radius of influence is not at an optimum value (750 km for the Cressman method), by far the largest decrease in the ageostrophic component results when the radar winds are averaged over longer time intervals. Successive scans do not appear to give an improvement over a single scan with the Cressman method when an optimum radius of influence is used for the single scan. Finally, a simple geostrophic wind calculation using three radiosonde stations within 500 km of the radar was competitive with the Cressman analysis when compared to a 12-hour average of the radar winds at stratospheric heights. In the troposphere the objective analysis methods provide a better estimate.

The results described here are not only important as an evaluation of the Cressman and Gandin schemes. They also have implications for the more sophisticated objective analysis methods described by Schlatter [1975] and Schlatter et al. [1976] for example. In general, the improvements on the simple schemes have involved using both an autocorrelation for the variables being interpolated and also crosscorrelations with the other observed variables. Thus the objective analysis method of Schlatter [1975] uses the

observed winds and the geostrophic wind relation to provide additional information for interpolating the height field. Therefore an analysis of the geostrophy of the wind, such as the one described here, will also be important for the more complex objective analysis methods.

We plan to describe the results presented here in a paper to be submitted to Monthly Weather Review. The second part of our study will involve a comparison of the radar winds with the analysis method of Schlatter [1975]. Finally, the estimates of the ageostrophic wind components derived from these comparisons with the objective analysis methods will be used to study geostrophic adjustment (see Blumen, 1972). We intend to use the radar data to determine if inertial waves generated during periods when large ageostrophic winds are present can be detected.

References

Balsley, B.B., and K.S. Gage, The MST radar technique: Potential for middle atmospheric studies, Pure Appl. Geophys., 118, 452-493, 1980.

Balsley, B.B., W.L. Ecklund, D.A. Carter, and P.E. Johnston, The MST radar at Poker Flat, Alaska, Radio Sci., 15, 213-224, 1980.

Cressman, G.P., An operational objective analysis system, Mon. Wea. Rev., 87, 367-374, 1959.

Gage, K.S. and B.B. Balsley, Doppler radar probing of the clear atmosphere, Bull. Amer. Met. Soc., 59, 1074-1093, 1978.

Gandin, L.S., Objective analysis of meteorological fields, translated from the Russian (1965) by the Israel Program for Scientific Translations Ltd., Jerusalem, 242 pp, 1963.

Kruger, H.B., General and special approaches to the problem of objective analysis of meteorological variables, Quart. J. Roy. Meteor. Soc., 95, 21-39, 1969.

Kruger, H.B., and J.M.R. Asselin, A statistical-dynamical objective analysis scheme, Supplement No. 1, Canadian Meteorological Memoirs No. 23, Meteorological Branch, Dept. of Transport., Toronto, 1967.

Otto-Bliesner, B., D.P. Baumhefner, T.W. Schlatter, and R. Bleck, A comparison of several meteorological analysis schemes over a data-rich region, Mon. Wea. Rev., 105, 1083-1091, 1977.

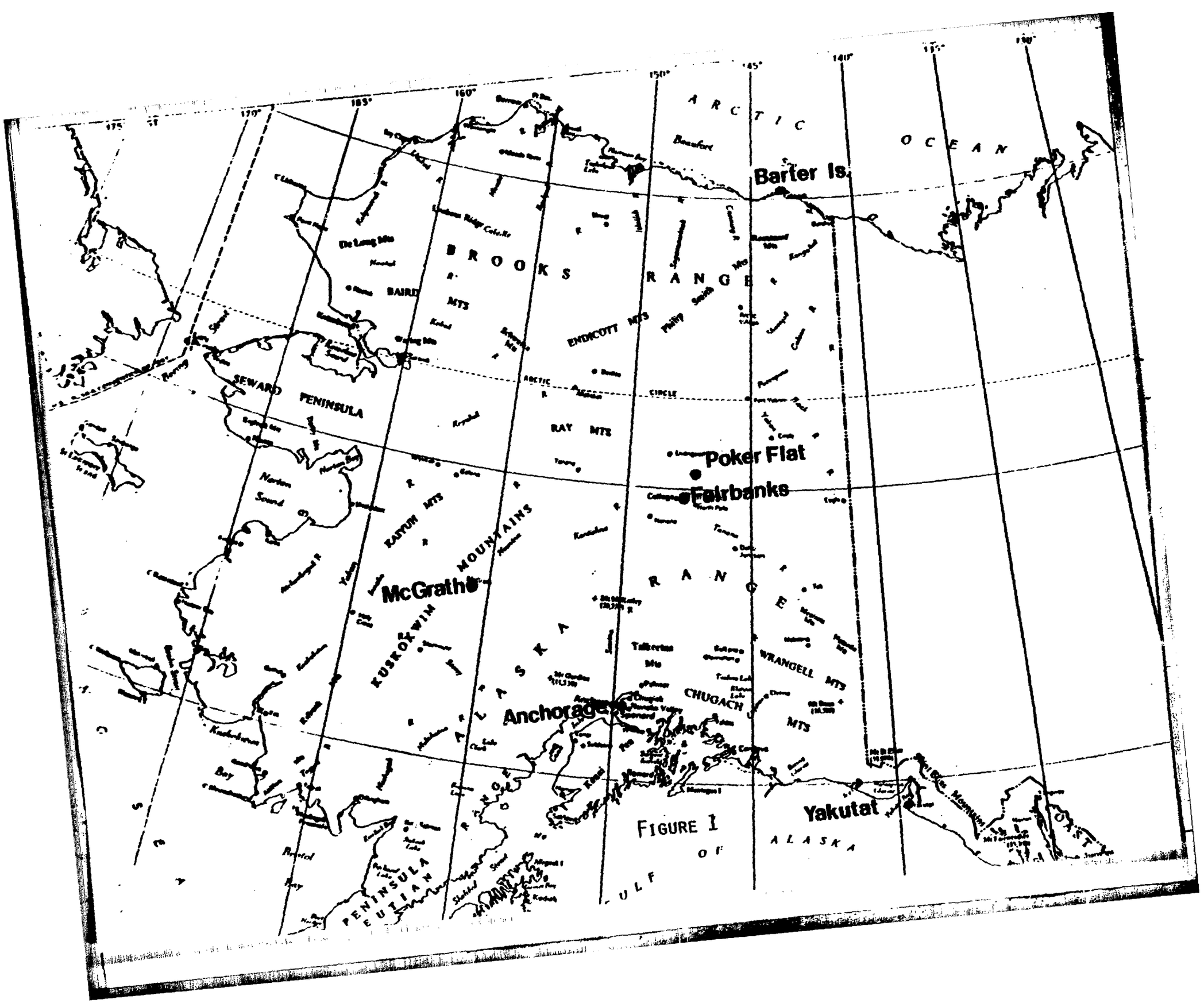
ARCTIC OCEAN
Barter Is.
BROOKS RANGE
BAIRD MTS
ENDICOTT MTS
SEWARD PENINSULA
ARCTIC CIRCLE
RAY MTS
Poker Flat
Fairbanks
KATUM MTS
KUSKOKWIM MOUNTAINS
McGrath
ALASKA RANGE
WRANGELL MTS
CHUGACH MTS
Anchorage
Yakutat
ALASKA
PENINSULA

FIGURE 1

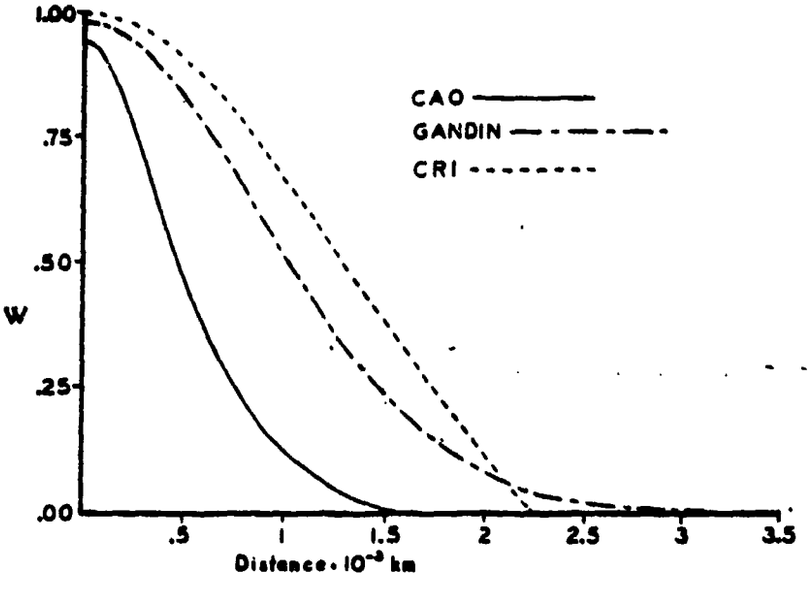

Figure 2. Weighting functions for three different objective analysis schemes. CRl is the Cressman method, GANDIN is the Gandin method which uses a Gaussian weighting, and CAO is the Central Analysis Office of Canada autocorrelation curve.

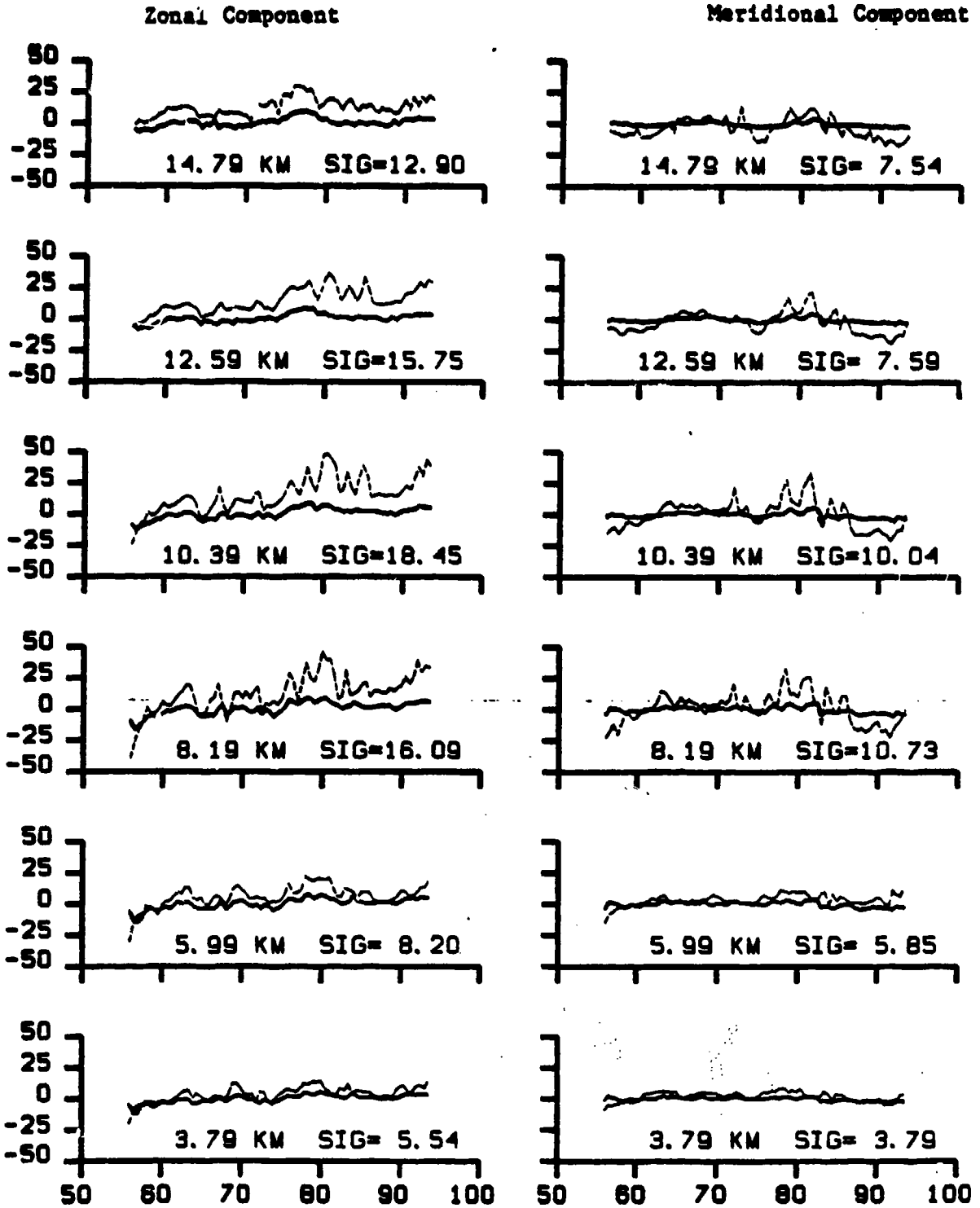

Figure 3a. Cressman analysis for the period from February 25 to April 3, 1979. The radius of influence used was 1,000 km. The heavy line shows the geostrophic wind calculated from the analyzed data. The light line shows the radar data averaged over 12 hours around the time indicated. The horizontal axis is Julian days.

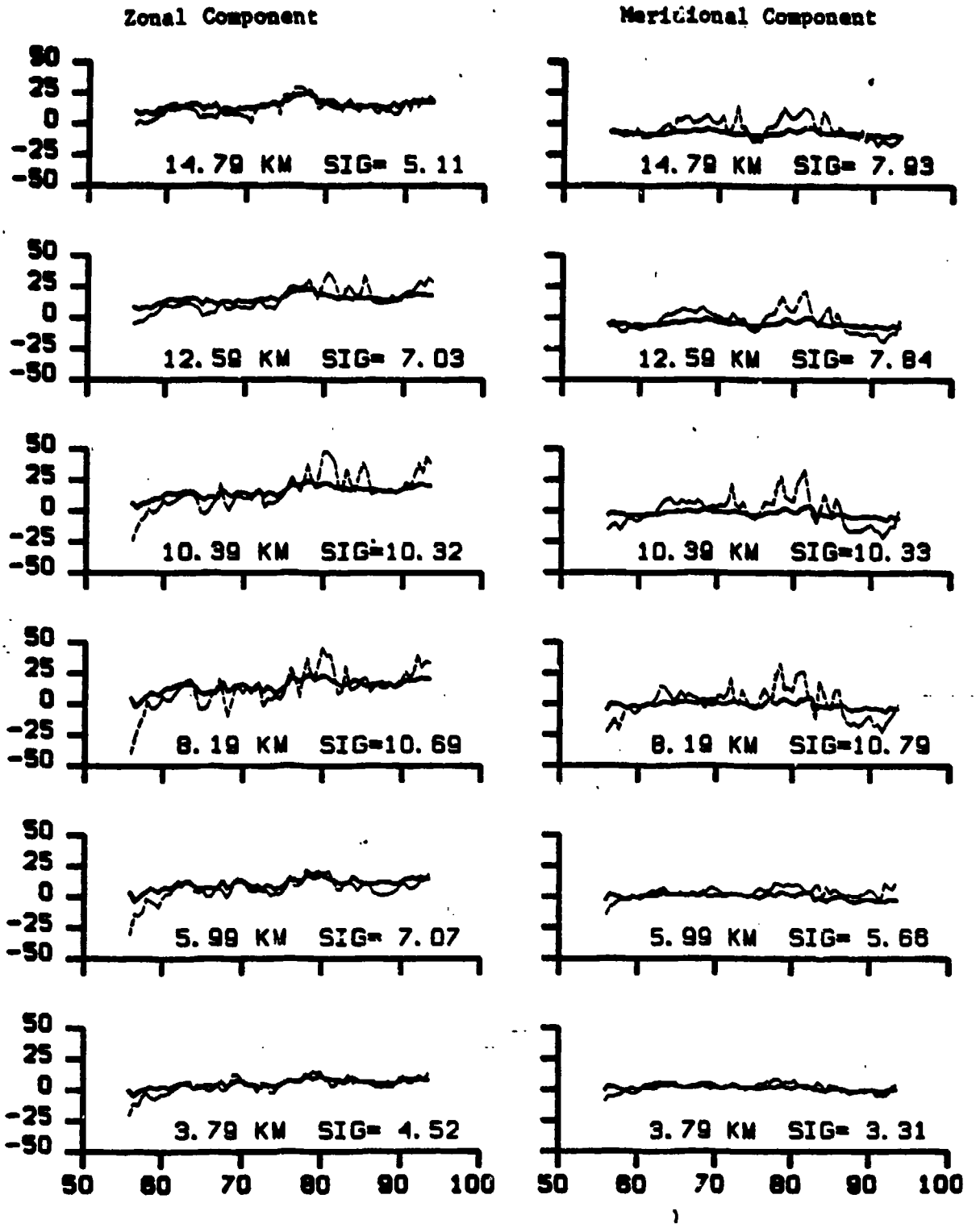

Figure 3b. Same as Figure 3a but with an improved initial estimate of the height field. The average heights at each of the observation points during the forty day period were used to calculate an estimated value at each of the grid points.

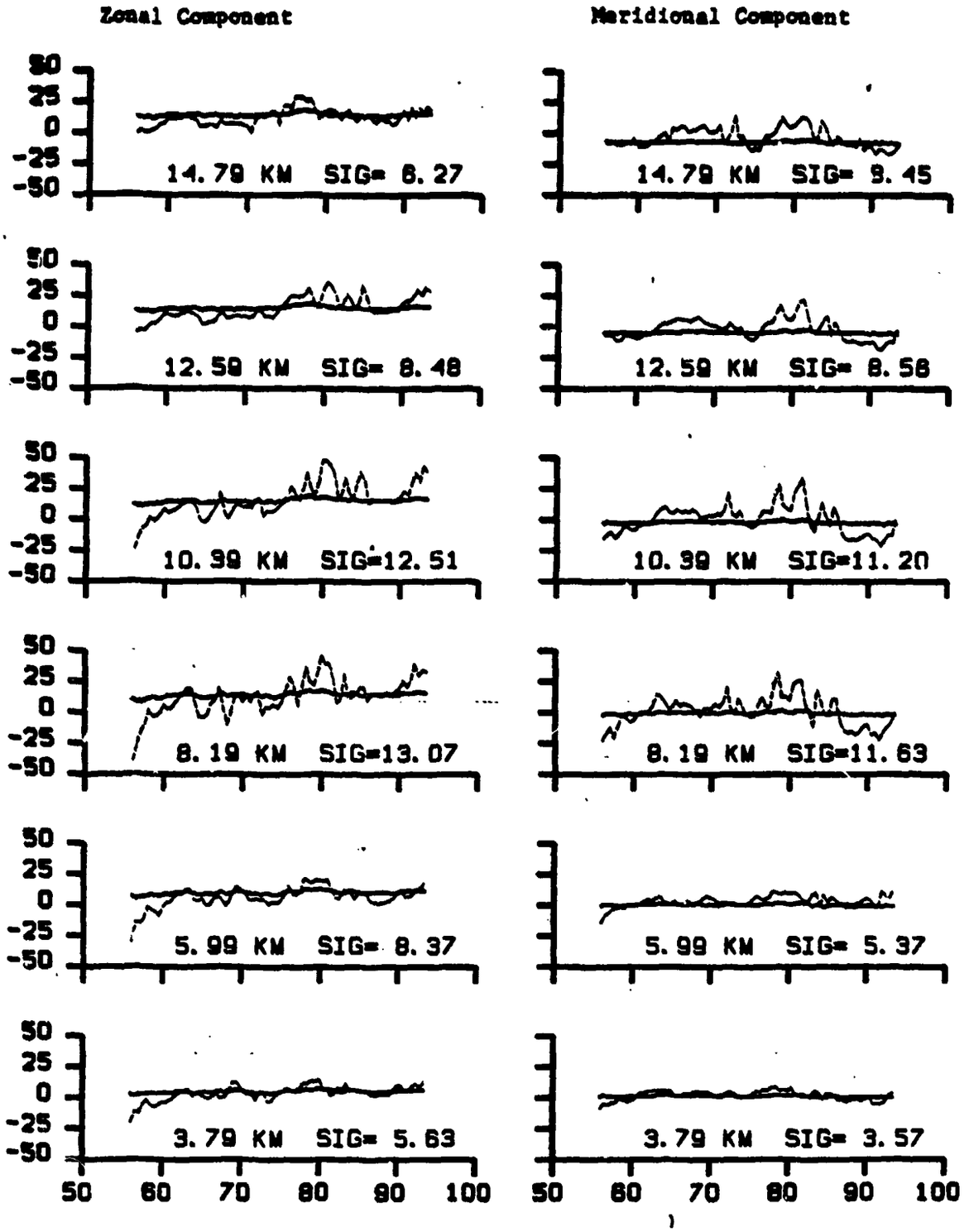

Figure 3c. Same as Figure 3b but with a radius of influence of 2,000 km.

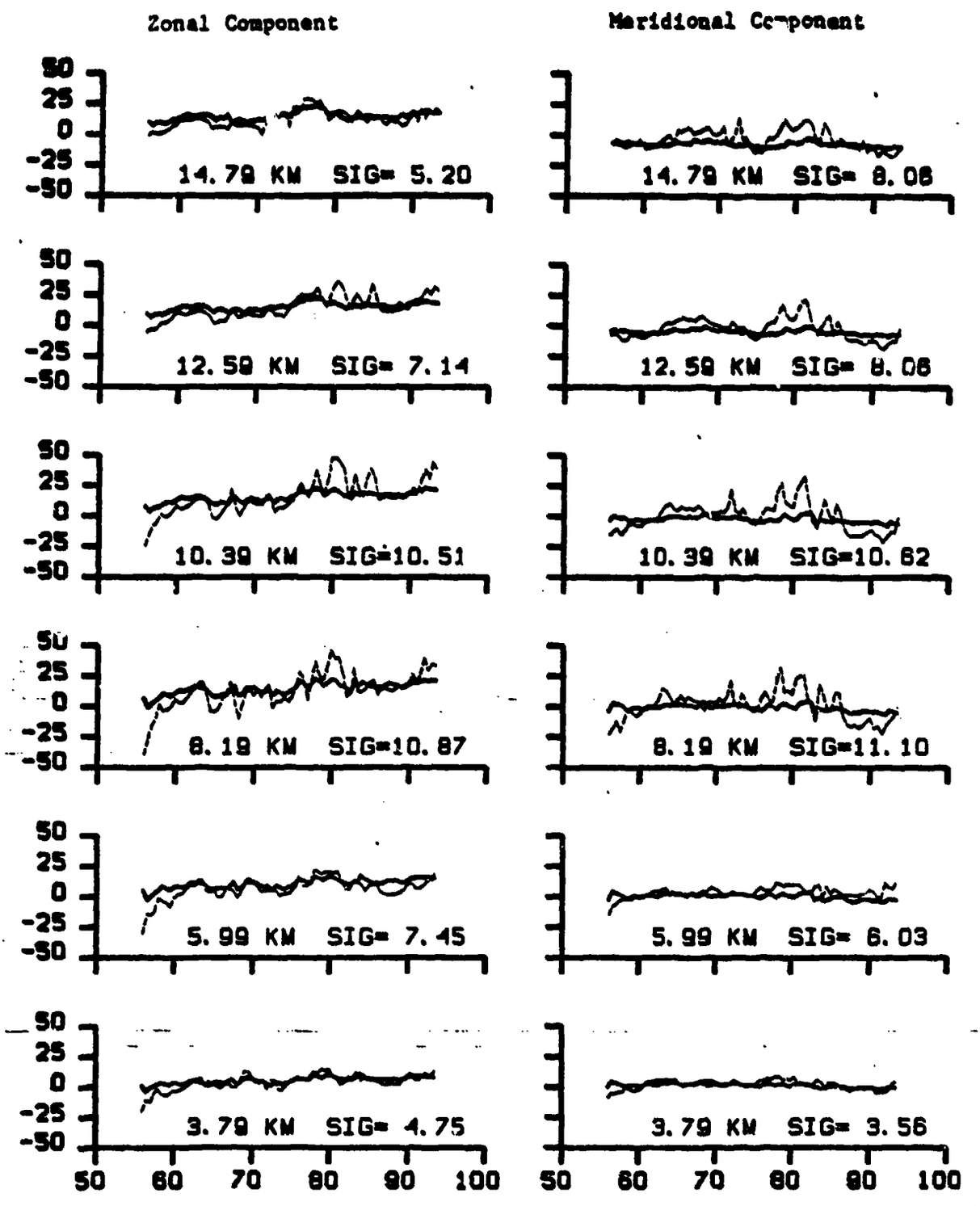

Figure 3d. Comparison of the Gandin objective analysis method with the 12-hour average radar winds. A Gaussian half-width of 500 km was used for the weighting function.

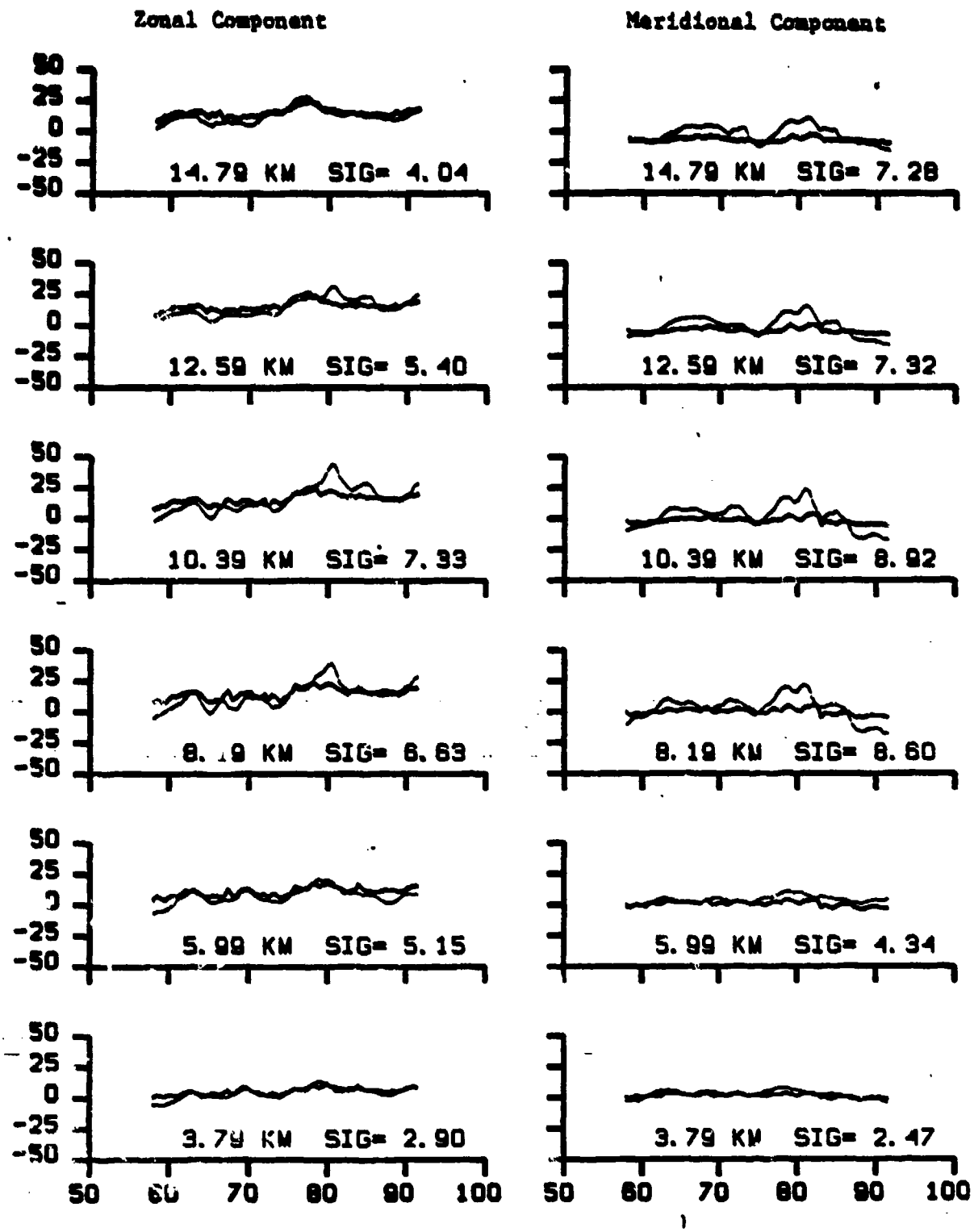

Figure 3e. Cressman analysis with a radius of influence of 1,000 km compared to a 48-hour average of the radar winds.

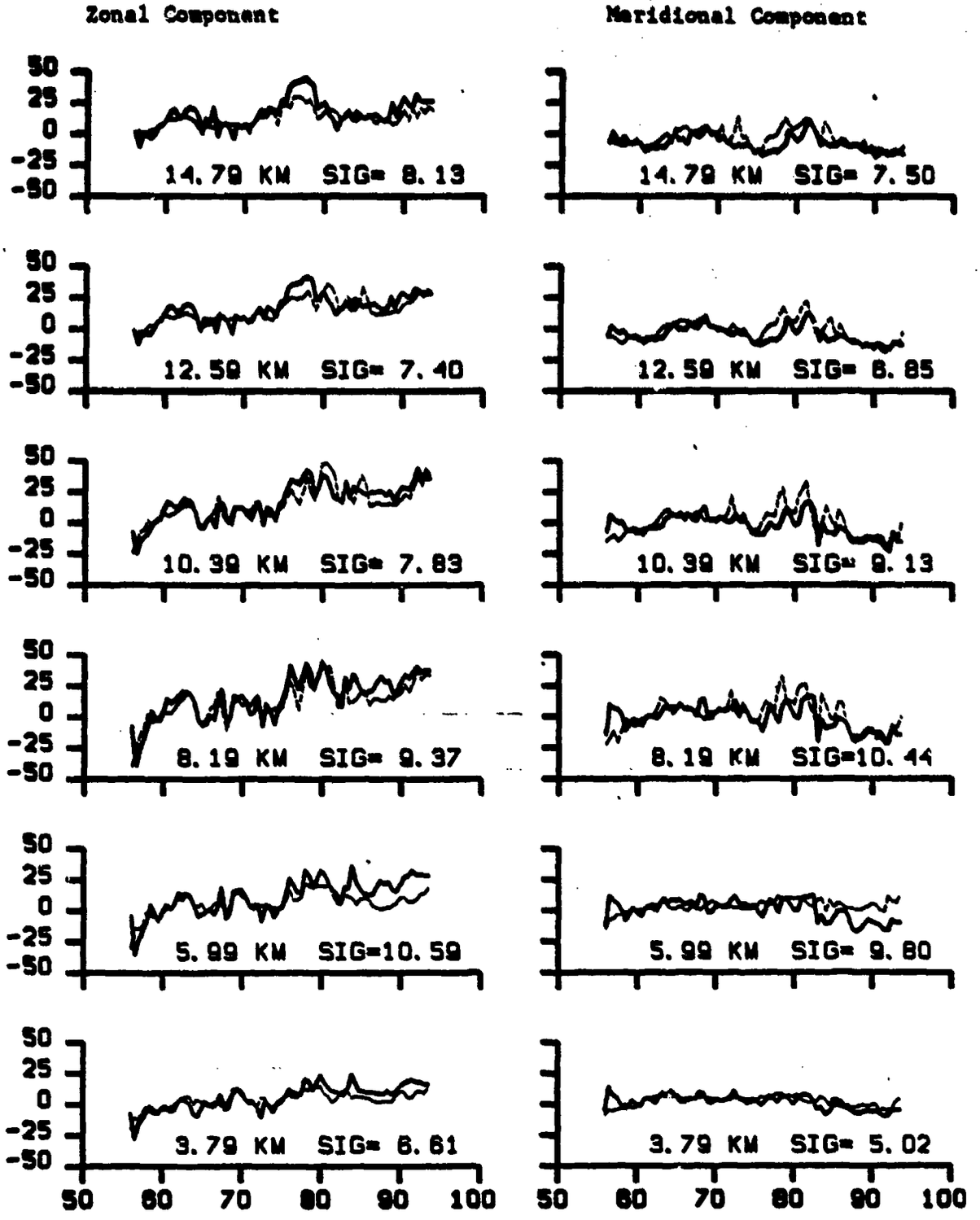

Figure 3f. Cressman analysis with five successive scans compared to 12-hour average of the radar winds. During the first scan the radius of influence is 2,000 km. On each successive scan the radius is decreased by 400 km.

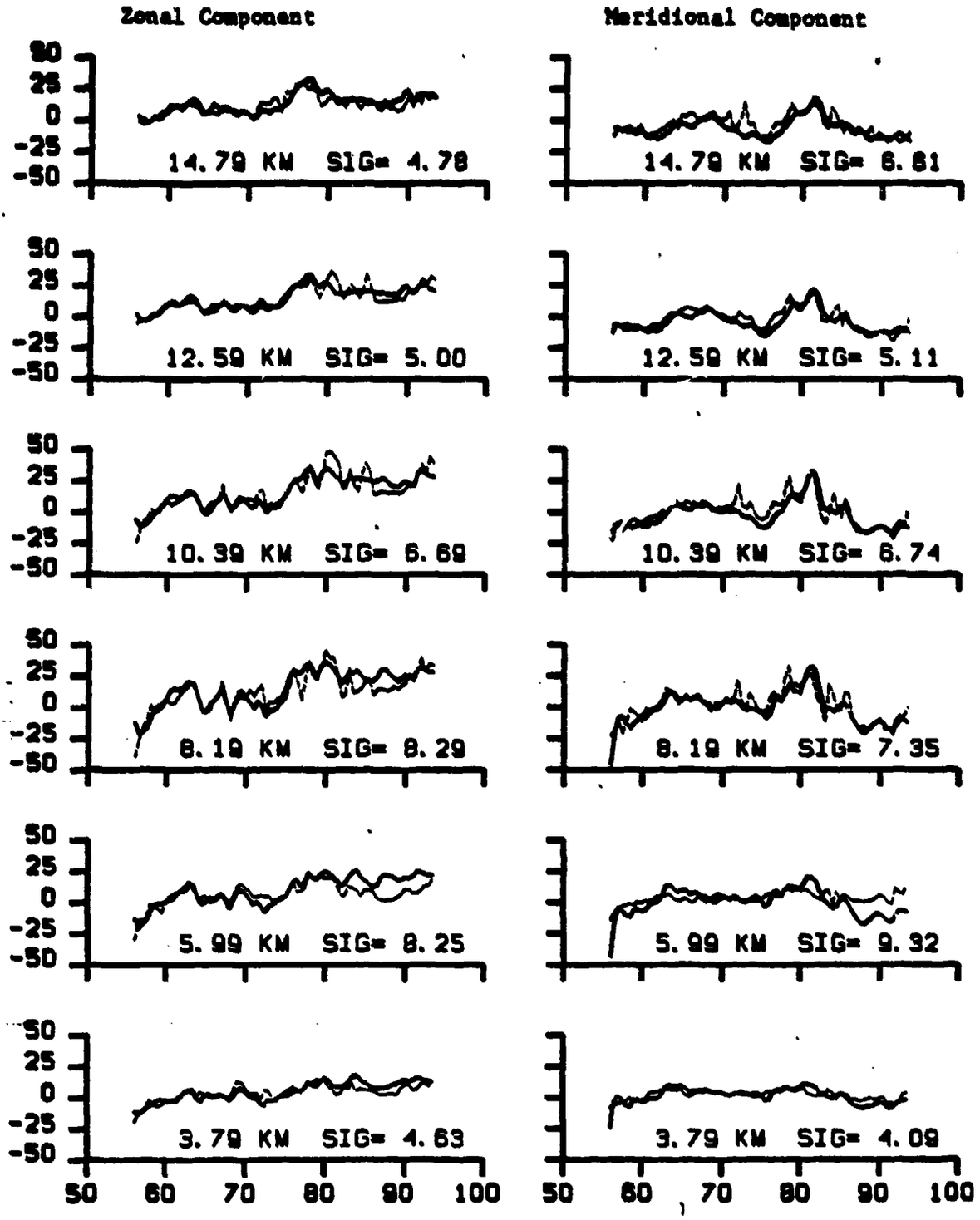

Figure 3g. The geostrophic wind determined by using the observations at McGrath, Fairbanks, and Anchorage compared to the 12 hour average of the radar winds. A three-point moving average has been applied to the geostrophic wind calculated from the radiosonde data.

APPENDIX

TURBULENCE SPECTRA IN THE UPPER TROPOSPHERE AND LOWER STRATOSPHERE AT PERIODS BETWEEN 2 HOURS AND 40 DAYS

Miguel Folkmar Larsen and Michael C. Kelley

Cornell University, Ithaca, New York 14850

K. S. Gage

Aeronomy Laboratory, NOAA, Boulder, Colorado 80303

Abstract. Zonal and meridional wind measurements made with the Poker Flat MST radar over a 40 day period are used to calculate the frequency power spectra at heights between 5.99 and 14.69 km. The winds used in the analysis are 1-hour averages of samples taken every 4 min. We find that the spectra follow an $f^{-5/3}$ power law in the range of periods from 2 to 50 hours. If the Taylor transformation is valid in this frequency range, this would imply a $k^{-5/3}$ wave number spectrum, corresponding to an inertial subrange for two-dimensional turbulence at the meteorological mesoscale. The implication of this result is that a source of energy exists at the high wave number end of the spectrum with energy flowing towards lower wave numbers.

1. Introduction

The study of atmospheric turbulence spectra is important for two reasons. First, the shape of the spectrum shows the position of the sources and sinks of energy and enstrophy and how nonlinear interactions distribute these quantities in a statistical sense. Second, the limits of predictability of the atmospheric state depend on the form of the wavenumber power law as shown by the work of Lorenz [1969] and Leith and Kraichnan [1972]. A large number of studies have been made with the aim of defining the frequency or wavenumber power laws. In general they fall into one of two categories, those dealing with large spatial and temporal scales utilizing radiosondes [Kao and Wendell, 1970; Kao and Lee, 1977; Julian et al., 1970] or superpressure balloons

[Mantis, 1970; Wooldridge and Reiter, 1970; Desbois, 1975]; and those dealing with small scales utilizing data from instrumented aircraft [Kao and Woods, 1964], meteorological towers or tethered balloons [Chernikov et al., 1969]. The part of the spectrum where little information has been available is in the meteorological mesoscale.

The mesoscale is characterized by periods between a few hours and a few days and spatial scales of 1000 km or less. Meteorological towers or tethered balloons are capable of resolving frequencies in this range but they cannot operate outside the planetary boundary layer. Since radiosondes are launched twice per day, the minimum frequency that can be resolved has a period of 1 day. This is at the outer edge of the mesoscale range. The superpressure balloons which are flown in the southern hemisphere have the potential for investigating subsynoptic scale motions [see e.g. Cadet, 1978] but until recently the temporal resolution has been on the order of a day due to problems of data storage and transmission.

The NOAA MST [Mesosphere/Stratosphere/Troposphere] radar located at Poker Flat, Alaska was put into routine operation in the first months of 1979. The system has been described in detail by Balsley et al. [1980], Gage and Balsley [1978], and Balsley and Gage [1980]. The radar uses the Doppler shift of signals back-scattered by turbulent fluctuations in the refractive index to measure line-of-sight velocities. By using three beams pointed in different directions, the complete profile of the vector winds can be determined. The time resolution is only limited by the integration time required to obtain a good signal-to-noise ratio. However, the fact that the Poker Flat radar is designed to operate unattended means that there is a practical limit imposed on the time resolution in order to avoid changing data tapes too often. For this reason the time between successive profiles is four minutes. In 1979 when the

data set described here was obtained, only a quarter of the full system had been completed. Thus the altitude range in which useful measurements could be obtained was limited to heights between 5.99 and 14.79 km. This time resolution and height range make the instrument ideal for investigating the power spectra of motions at synoptic and mesoscales.

2. Description of the Data Set and Spectral Analysis

During the time from February 23 to April 5, 1979 the Poker Flat radar was operated in a mode with two beams at 15° off-vertical, one pointed roughly north and the other roughly east. Computing limitations excluded the possibility of operating a third, vertically-pointing beam during that time although this situation has been rectified since then. For this original data set it was assumed that the entire contribution to the line-of-sight velocities was due to a horizontal wind vector. The antenna consisted of a 100 m^2 phased dipole array, one-fourth the size the array will have upon completion. Sixteen 100 kW transmitters were used, giving a peak transmitted power of 0.8 MW per beam. This configuration together with a 15 μs pulsewidth provided one complete profile every 4 min up to an altitude of 14.69 km and a height resolution of ~2.2 km.

Coherent integrations and the Fast Fourier Transforms of the received signals are done on line. The spectra are then processed at the Aeronomy Lab in Boulder, Colorado. The processing scheme is described in Carter et al. [1980] and provides line-of-sight Doppler shifts at each height. The assumption that the entire contribution to the line-of-sight velocities is due to a horizontal wind vector is an increasingly good assumption as the averaging interval is increased. One way to understand this is to consider the polarization relations for gravity waves in an isothermal atmosphere (given by Beer [1974] for instance). The requirement for the validity of the hydrostatic

approximation turns out to be that $\omega^2 << \omega_b^2$, where ω is the angular frequency of the motion and ω_b is the Brunt-Vaisala period. For periods of half an hour or more the contribution from the vertical velocity component is certainly negligible. However for samples taken at intervals less than this, the vertical velocity component can contribute significantly. To avoid problems of this type, the 4 min data was averaged over one-hour intervals centered on the full hour. The data thus consists of 42 days of one-hour average horizontal winds. For this study 40 of the days were used, yielding a time series of 960 points.

The time series was treated in several ways before the spectra were calculated. First, missing data points were replaced by interpolating between adjacent points. The number of missing points was less than 45, out of the total of 960, for the heights discussed here. Above 14.69 km and below 5.99 km data was also available, but the number of missing points was approximately four times as large. After the missing data points were replaced by the interpolated values the mean was calculated and subtracted. Then a Hanning window was applied, affecting 96 or 10% of the points at each end of the series. The Hanning window helps to eliminate energy spillage from the low frequency end of the spectrum into the high frequency end as a result of broadening due to discrete sampling.

The original data is shown in Figure 1. The five curves at the top of the figure are for the zonal wind, and the curves at the bottom are for the meridional component. The data that is shown has not been treated in any way. Both the average for the entire time series at each height and the variance are given below the corresponding curve. Each time series was screened for occurrences of wind variations greater than 7 m/s between adjacent points. In almost all cases where variations larger than this occurred a large change in

the wind component was found both preceding and following the questionable data point. A data point such as this was considered to be erroneous and replaced by the interpolated value. Removing these erroneous data points decreased the amount of variability in the high frequency end of the computed power spectra.

The Fourier transform was computed with an algorithm described by Singleton [1967]. This routine has the advantage that the number of points does not have to be a power of 2. After the spectrum was calculated it was smoothed by the function

$$P(i) = 1/64\ (P(i-3) + 6P(i-2) + 15P(i-1) + 20P(i) + 15P(i+1) + 6P(i+2) + P(i+3)) \quad (1)$$

as suggested by Endlich et al. [1969]. The smoothing decreases the resolution but increases the statistical stability.

3. Frequency spectra and wind variances

The resulting spectra are shown in Figures 2a and 2b. Figure 2a represents the spectra for the zonal component at the five heights, and Figure 2b shows the corresponding spectra for the meridional component. Spectra at succesive heights have been multiplied by a factor of 100 to separate them on the graph. The units for the two spectra at 5.99-km altitude are correct. Least-squares fits of a function of the form

$$P(f) = P_o\ (f/f_o)^n$$

were made to determine the spectral index n. Here P is the power, and f is the frequency. The calculated value of n is shown next to the corresponding curve in Figures 2a and 2b. A dashed line is used to show the fit. The least-squares computation was carried out for frequencies in the range from $f = 0.015$ hr^{-1} to $f = 0.45$ hr^{-1}. The average value of the spectral index for the zonal component is -1.604 ± 0.279. The average value of the index for the

meridional component is -1.604 ± 0.259. The value of -1.604 is very close to $-5/3$. There is no particular reason to expect an $f^{-5/3}$ power law; however, if the Taylor transformation is valid in this range of frequencies, then a $k^{-5/3}$ power law is implied. This would correspond to an inertial subrange. There is no independent evidence from this study to indicate whether the Taylor transformation, i.e., that temporal scales are related to spatial scales by a constant factor of the mean wind over the sampling time, is valid. However, the results of a study by Brown and Robinson [1979] in which European radiosonde data was used were that the Taylor transformation can be used for spatial scales smaller than 1200 km and at least down to 200 km, the lower limit of the resolution of the network they used. The corresponding range of periods where the transformation was valid was in the range less than 2 days.

Gage [1979] summarized the diverse evidence for the existence of a $k^{-5/3}$ law inertial range at the meteorological mesoscale. He also used the variability calculated from a 7 hour, high resolution, balloon wind measurement experiment and wind measurements made with the Sunset VHF Doppler radar in Colorado over a 14 hour period to show that the variance defined by

$$\sigma_\tau = \overline{\{[v(t)-v(t+\tau)]^2\}}^{1/2} \qquad (2)$$

follows a $\tau^{+1/3}$ power law out to time lags of at least 3 to 5 hours. This is consistent with a $k^{-5/3}$ power law when the Taylor transformation is valid as shown by Gage [1979].

Plots of the variance σ_τ are presented in Figures 3a and 3b for the zonal and meridional wind components respectively. Lines with slopes of +1/3 are superimposed on the curves for reference. Successive curves have been multiplied by a factor of ten to separate them on the graph. The scale is correct for the variance curve at 10.39-km altitude. Overall, the 1/3 slope

gives a reasonable fit to the curves. However, there is a pronounced "bump" with a peak near 25 hours at 8.19, 10.39, and 12.59 km which is particularly noticeable in the zonal wind component. This peak in the variance should not be confused with a diurnal effect since a peak in the variance at 25 hours, for instance, will correspond to a frequency with a period of 50 hours. This can be seen in the spectra shown in Figures 2a and 2b. A unique feature of the curves for the meridional wind is the rapid decrease in the variance for lags greater than 600 hours or 25 days.

5. Discussion

In the preceding section it was shown that the frequency spectra for motions with periods in the range of 2 hours out to periods around 50 hours generally follow a -5/3 power law. Kao and Wendell [1970], Kao and Lee [1979], Wooldridge and Reiter [1970] and others have used temporal and spatial transforms of radiosonde data to show that at the synoptic scale, frequency power spectra follow a -1 power law while wavenumber power spectra follow a -3 power law. Periods of 2 to 3 days are at the high frequency limit of these studies. Indeed, it may be argued that there is some hint of a change to a slope of -1 at periods near 50 hours in the spectra shown in Figures 2a and 2b. The -1 slope frequency range, corresponding to the -3 wavenumber regime, is consistent with a region on the high wavenumber side of a source of enstrophy, presumably the baroclinic instability, with enstrophy cascading toward larger wavenumbers [Kraichnan, 1967]. Gage [1979] pointed out that at the meteorological mesoscale, characteristic scale sizes are too large for three-dimensional turbulence to exist. If a -5/3 inertial subrange is present and if it is associated with two-dimensional turbulence, then it will be characterized by an energy source at higher wavenumbers, with energy propagating up the spectrum toward lower wavenumbers, as shown by Kraichnan

[1967]. Since a three-dimensional inertial subrange is also characterized by a -5/3 power law but has the energy source at lower wavenumbers with energy propagating toward higher wavenumbers, it is important to know if the flow is really two- or three-dimensional. Gage [1979] argued that the validity of the hydrostatic approximation at time scales corresponding to the frequency range studied here would be an argument in favor of the two-dimensionality of the flow. We can also consider the work of Charney [1971]. He was able to show that the constraints imposed on two-dimensional turbulence, i.e., conservation of both energy and enstrophy, also appear if the flow is quasi-geostrophic. Therefore, it is not an inherent lack of variability of the flow in the vertical direction, but rather the geostrophy of the flow, that makes the two-dimensional turbulence theory applicable. A study by Larsen and Kelley [1980] using the same data base discussed in this paper indicates that the geostrophic approximation is reasonable for winds averaged over periods of half a day or less. This result also argues in favor of the applicability of the two-dimensional rather than the three-dimensional turbulence theory for flow at the meteorological mesoscale. Since the theoretical work of Kraichnan [1967] has also shown that enstrophy cannot propagate through a region characterized by a -5/3 power law, and energy cannot propagate through a region characterized by -3 power law, this implies that there must be a sink of energy and enstrophy at the break in the spectrum. In our case the break appears at periods near 50 hours. Using the mean value of the zonal wind over the 40 day period, this frequency converts to a scale size of roughly 1800 km. In his study Gage found that the break occurs at scale sizes around 1000 km. The physical picture outlined here is summarized in Figure 3 which shows the various power laws, direction of flow of energy and enstrophy, and sources and sinks at their locations relative to changes of slope in the spectrum.

6. Conclusion

The Poker Flat MST radar has provided a high time resolution data series of horizontal winds over a 40 day period. Spectral analysis of these winds indicates that the two-dimensional inertial energy subrange discussed by Gage [1979] does exist at the meteorological mesoscale. This result together with results of earlier studies of power spectra for synoptic scale motions implies that sources of energy and enstrophy are present at both large and small scales. The large scale source is presumably due to instabilities of planetary-scale waves. At the small-scale end of the spectrum the energy source is characterized by periods less than 2 hours. Theoretical considerations imply that a sink of energy and enstrophy must exist at the break between the synoptic and mesoscale. This sink is characterized by periods of approximately two days and scale sizes of 1000 to 2000 km.

Acknowledgements: We are indebted to B. B. Balsley, D. Carter, and W. Ecklund for all their work in obtaining the data, their helpfulness in furnishing it to us, and their willingness to discuss various aspects of it with us. We also thank T. Riddle for his efforts in generating the actual data tapes that we used. This research was supported by grant AFOSR-80-0020.

References

Balsley, B. B., and K. S. Gage, The MST radar technique: Potential for middle atmospheric studies, Pure Appl. Geophys., 118, 452-493, 1980.

Balsley, B. B., W. L. Ecklund, D. A. Carter, and P. E. Johnston, The MST radar at Poker Flat, Alaska, Radio Sci., 15, 213-224, 1980.

Beer, T., Atmospheric Waves , John Wiley and Sons, New York, 1974.

Cadet, D., The superpressure balloon sounding technique for the study of atmospheric meso- and microscale phenomena, Bull. Am. Met. Soc., 59, 1119-1127, 1978.

Carter, D. A., B. B. Balsley, and W. L. Ecklund, The Poker Flat MST radar: Signal analysis and data processing techniques with examples, Preprints of 19th Conference on Radar Meteorology, AMS, 45 Beacon St., Boston, Mass. 02108, 1980.

Chernikov, A. A., Y. V. Mel'nichuk, N. Z. Pinus, S. M. Shmeter, and N. K. Vinnichenko, Investigations of the turbulence in a convective atmosphere using radar and aircraft, Radio Sci., 1257-1259, 1969.

Desbois, M., Large-scale kinetic energy spectra from Eulerian analysis of Eole wind data, J. Atmos. Sci., 32, 1838-1847, 1975.

Endlich, R. M., R. C. Singleton, and J. W. Kaufman, Spectral analysis of detailed vertical wind speed profiles, J. Atmos. Sci., 26, 1030-1041, 1969.

Gage, K.S. and B.B. Balsley , Doppler radar probing of the clear atmosphere, Bull. Amer. Met. Soc., 59, 1074-1093, 1978.

Gage, K. S., Evidence for a $k^{-5/3}$ law inertial range in mesoscale two-dimensional turbulence, J. Atmos. Sci., 36, 1950-1954, 1979.

Julian, P. R., W. M. Washington, L. Hembree, and C. Ridley, On the spectral distribution of large-scale atmospheric kinetic energy, J. Atmos. Sci.,

27, 376-387, 1970.

Kao, S.-K., and H. N. Lee, The non-linear interactions and maintenance of the large-scale moving waves in the atmosphere, J. Atmos. Sci., 34, 471-485, 1977.

Kao, S.-K., and L. L. Wendell, The kinetic energy of the large-scale atmospheric motion in wavenumber-frequency space, I. Northern hemisphere, J. Atmos. Sci., 27, 359-375, 1970.

Kao, S.-K., and H. D. Woods, Energy spectra of meso-scale turbulence along and across the jet stream, J. Atmos. Sci., 21, 513-519, 1964.

Kraichnan, R. H., Inertial ranges in two-dimensional turbulence, Phys. Fluids, 10, 1417-1423, 1967.

Larsen, M. F. and M. C. Kelley, Report on the Analysis of Data from the NOAA/Alaskan MST Radar System, Report to AFOSR, School of Electrical Engineering, Cornell University, Ithaca, NY 14853, 1980.

Leith, C. E., and R. H. Kraichnan, Predictability of turbulent flows, J. Atmos. Sci., 29, 1041-1058, 1972.

Lorenz, E. N., The predictability of a flow which possesses many scales of motion, Tellus, 21, 289-307, 1969.

Mantis, H. T., The structure of winds of the upper troposphere at mesoscale, J. Atmos. Sci., 20, 94-106, 1963.

Singleton, R. C., On computing the fast Fourier transform, Comm. A.C.M., 10(10), 647-654, 1967.

Wooldridge, G., and E. R. Reiter, Large-scale atmospheric circulation characteristics as evident from Ghost balloon data, J. Atmos. Sci., 27, 183-194, 1970.

Figure Captions

Figure 1. This shows the original data set of 960 hourly values at each of the five heights used in the study. The average value and the variance at each of the heights are shown. The top half of the figure shows the zonal wind component, and the bottom half shows the meridional component.

Figure 2a. These are the power spectra for the time series of the zonal component shown in the previous figure. The parameter n at the right of each spectrum is the least-squares fit value of the spectral index. The average value of the spectral index is -1.604 ± 0.279. Spectra at successive heights have been multiplied by a factor of 100 to separate them on the graph. The axes are correct for the spectrum at 5.99 km.

Figure 2b. Same as figure 2a but for the meridional wind component. The average value of the spectral index is -1.604 ± 0.259.

Figure 3a. This shows the variance of zonal wind as a function of the lag. The variance is defined in the text. Curves at successive altitudes have been multiplied by a factor of 10 to separate them on the graph. The vertical axis labeling is correct for the variance at 10.39-km altitude.

Figure 3b. Same as figure 3a but for the meridional wind component.

Figure 4. This graph illustrates the wave number power laws that are discussed in the text. The direction of the flow of energy and enstrophy are shown together with the various sources and sinks.

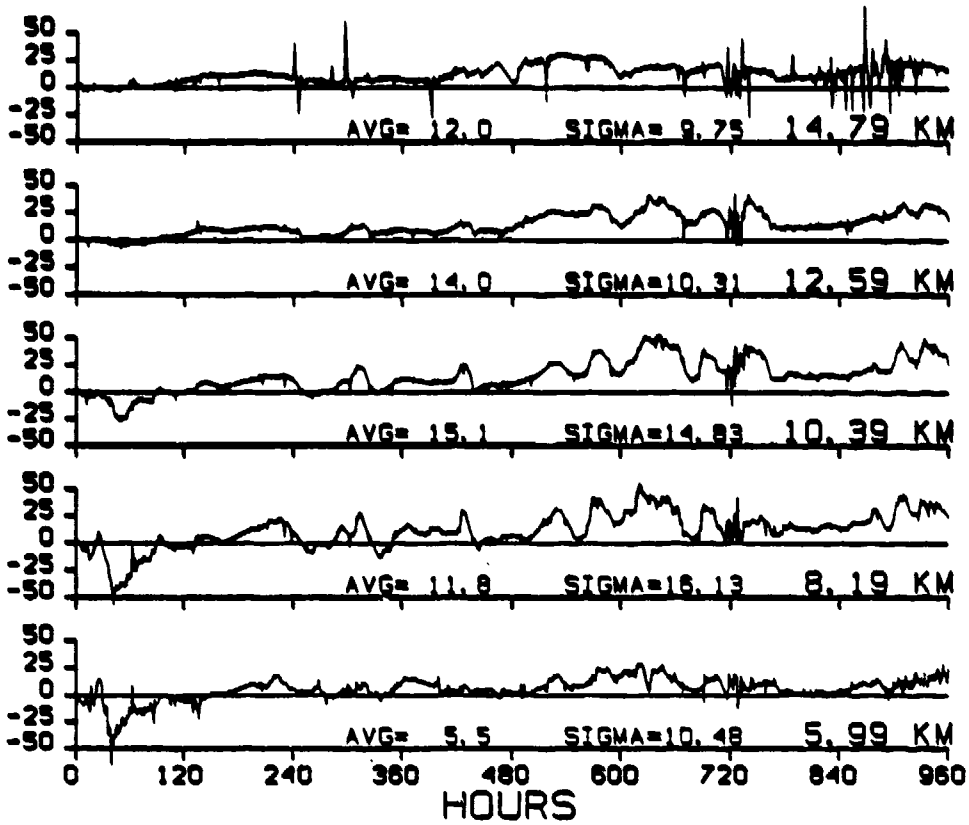
50
25
0
-25
-50
AVG= 12.0 SIGMA= 9.75 14.79 KM
AVG= 14.0 SIGMA=10.31 12.59 KM
AVG= 15.1 SIGMA=14.83 10.39 KM
AVG= 11.8 SIGMA=16.13 8.19 KM
AVG= 5.5 SIGMA=10.48 5.99 KM
0 120 240 360 480 600 720 840 960
HOURS

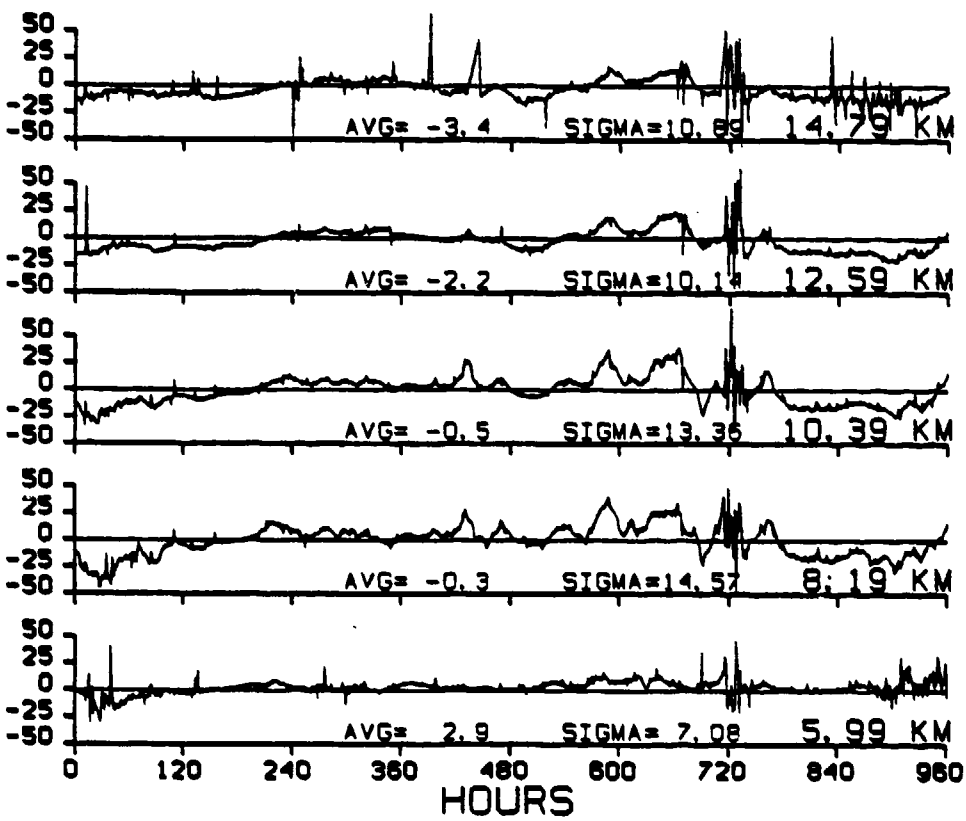
50
25
0
-25
-50
AVG= -3.4 SIGMA=10.89 14.79 KM
AVG= -2.2 SIGMA=10.14 12.59 KM
AVG= -0.5 SIGMA=13.36 10.39 KM
AVG= -0.3 SIGMA=14.57 8.19 KM
AVG= 2.9 SIGMA= 7.08 5.99 KM
0 120 240 360 480 600 720 840 960
HOURS

Figure 1

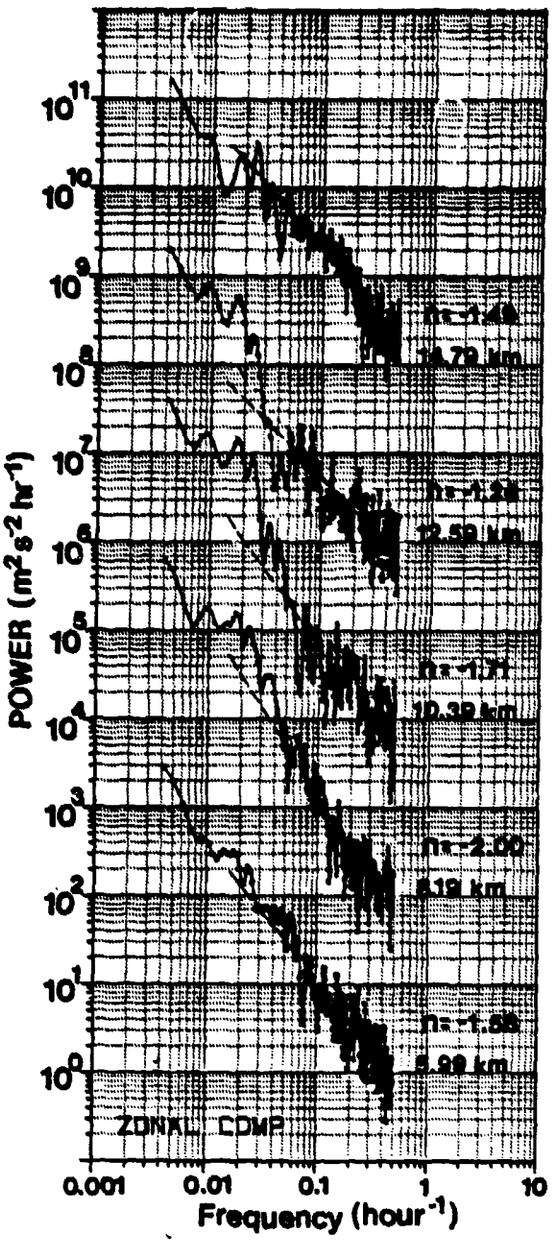
POWER ($m^2 s^{-2} hr^{-1}$)
10^{11}
10^{10}
10^{9}
10^{8}
10^{7}
10^{6}
10^{5}
10^{4}
10^{3}
10^{2}
10^{1}
10^{0}
n=-1.48
6.79 km
n=-1.28
2.59 km
n=-1.71
10.39 km
n=-2.00
3.19 km
n=-1.58
5.99 km
ZONAL COMP
0.001
0.01
0.1
1
10
Frequency ($hour^{-1}$)

Figure 2a

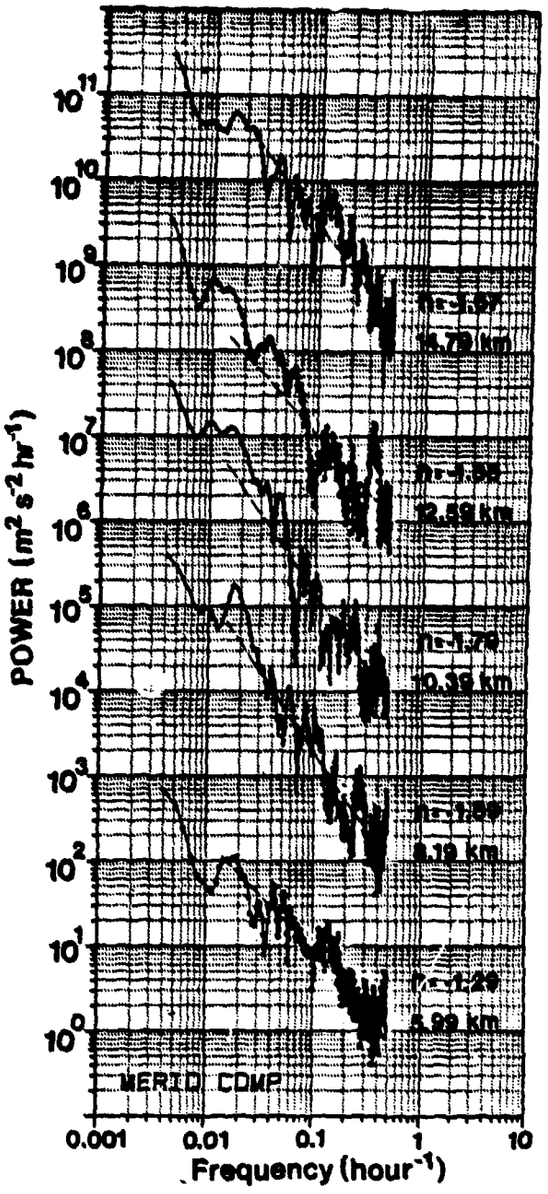
POWER ($m^2 s^{-2} hr^{-1}$)
10^{11}
10^{10}
10^{9}
10^{8}
10^{7}
10^{6}
10^{5}
10^{4}
10^{3}
10^{2}
10^{1}
10^{0}
MERID COMP
0.001
0.01
0.1
1
10
Frequency ($hour^{-1}$)

Figure 2b

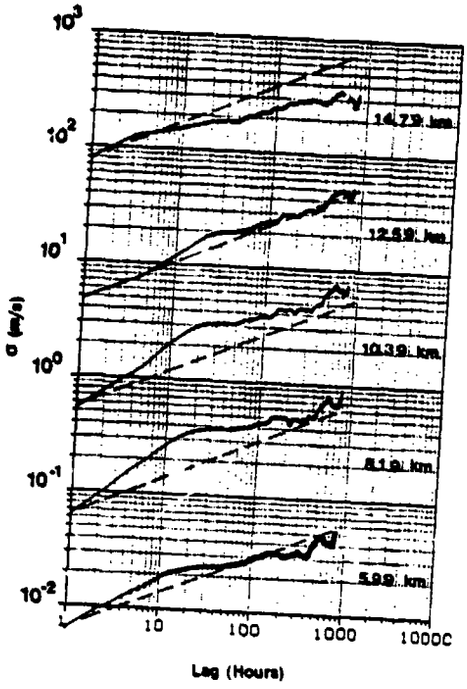

Figure 3a

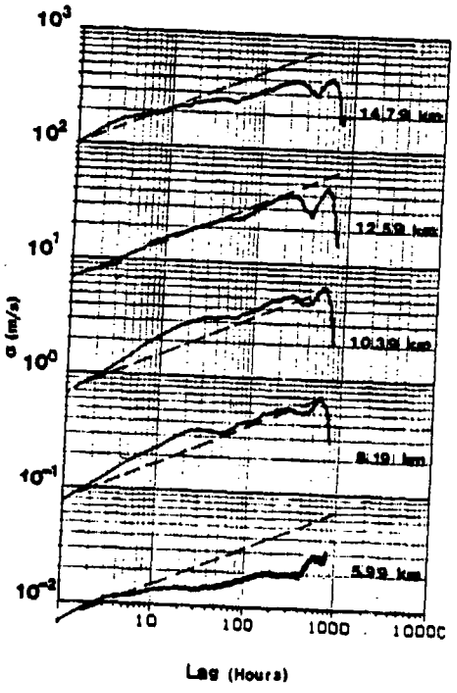

Figure 3b

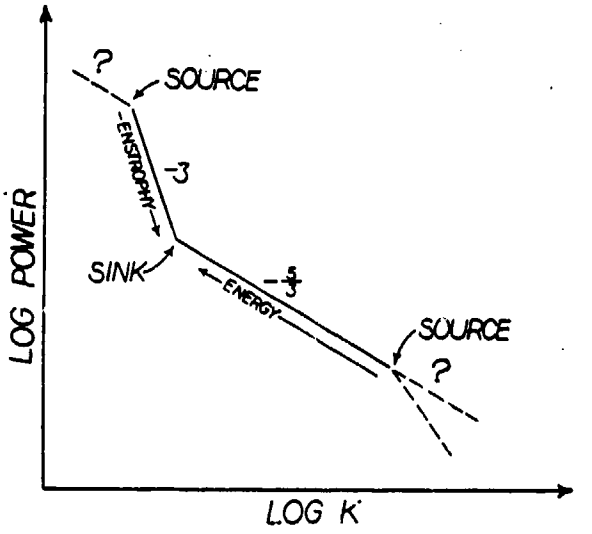

Figure 4